Original Article

JCBFM

Journal of Cerebral Blood Flow & Metabolism
0(00) 1–13

DOI: 10.1177/0271678X16686987
journals.sagepub.com/home/jcbfm
SAGE

Intraoperative multi-exposure speckle imaging of cerebral blood flow

Lisa M Richards[1], SM Shams Kazmi[1], Katherine E Olin[1], James S Waldron[2], Douglas J Fox Jr[2] and Andrew K Dunn[1]

Abstract

Multiple studies have demonstrated that laser speckle contrast imaging (LSCI) has high potential to be a valuable cerebral blood flow monitoring technique during neurosurgery. However, the quantitative accuracy and sensitivity of LSCI is limited, and highly dependent on the exposure time. An extension to LSCI called multi-exposure speckle imaging (MESI) overcomes these limitations, and was evaluated intraoperatively in patients undergoing brain tumor resection. This clinical study ($n = 8$) recorded multiple exposure times from the same cortical tissue area spanning 0.5–20 ms, and evaluated images individually as single-exposure LSCI and jointly using the MESI model. This study demonstrated that the MESI estimates provided the broadest flow sensitivity for sampling the flow magnitude in the human brain, closely followed by the shorter exposure times. Conservation of flow analysis on vascular bifurcations was used to validate physiological accuracy, with highly conserved flow estimates (<10%) from both MESI and 1 ms LSCI ($n = 14$ branches). The MESI model had high goodness-of-fit with proper image calibration and acquisition, and was used to monitor blood flow changes after tissue cautery. Results from this study demonstrate that intraoperative MESI can be performed with high quantitative accuracy and sensitivity for cerebral blood flow monitoring.

Keywords

Cerebral blood flow, intraoperative imaging, laser speckle contrast imaging, multi-exposure speckle imaging, neurosurgery

Received 18 July 2016; Revised 4 November 2016; Accepted 29 November 2016

Introduction

The brain relies on a constant supply of cerebral blood flow (CBF) to maintain normal function. Any prolonged reduction in CBF puts the patient at risk for ischemic brain injury, which can lead to neurologic deficits. CBF monitoring during neurosurgery is critical to warn surgeons about abnormal changes in blood flow, and can help minimize post-operative complications by enabling and guiding potential life-saving interventions.[1] Optical techniques based on coherent dynamic light scattering have the potential to meet this clinical need, providing a noninvasive, label-free, and continuous CBF monitoring solution. Laser speckle contrast imaging (LSCI) provides 2D full-field blood flow maps with high spatial resolution in real-time using very simple instrumentation that includes a low-power laser diode, imaging optics, and a camera, enabling noninvasive and non-contact imaging. Multiple studies have examined the use of LSCI during neurosurgical procedures, including surgical revascularization,[2–4] awake functional mapping,[5] and brain tumor resection.[6,7] LSCI has also been used to visualize cortical spreading depression[8] and to predict cortical infarction[9] during decompressive craniectomy for malignant stroke. All of these studies have shown the potential of LSCI as a useful CBF monitoring tool during neurosurgery.

[1]Department of Biomedical Engineering, The University of Texas at Austin, Austin TX, USA
[2]NeuroTexas Institute, St. David's Medical Center, Austin, USA

Corresponding author:
Andrew K Dunn, Department of Biomedical Engineering, University of Texas at Austin, 107 W. Dean Keeton Street C0800, Austin, TX 78712, USA.
Email: adunn@utexas.edu

One of the main limitations of LSCI has been its limited quantitative flow and perfusion accuracy reflecting the true physiological state, exhibited by high deviation and weak correlation with *in vivo* absolute flow velocities in animal studies.[10] This inaccuracy stems from the fact that traditional LSCI systems image CBF using a single camera exposure time, which limits flow sensitivity to a small range. In addition, single-exposure LSCI is sensitive to various instrumentation factors, including illumination variations, noise across imaging sessions, and variations in the proportion of dynamic versus static scattering contributions in the recorded light. This limits LSCI to intra-patient usage at a single time point, and prevents the establishment of quantitative thresholds needed to assist in surgical decision-making. An extension to LSCI called multi-exposure speckle imaging (MESI) has been developed that improves upon many of the shortcomings of LSCI, especially the quantitative accuracy.[11] MESI has been shown to be reliable for chronic imaging and to have high correlation with *in vivo* absolute velocities in animal studies,[10] suggesting potential for accurate intra- and inter-patient comparisons. The MESI technique records images at multiple exposure times to increase the sensitivity range of the instrument, and uses a more robust mathematical model utilizing the dependence on camera exposure to estimate flow with higher accuracy.[11]

Previous clinical studies have performed single-exposure LSCI intraoperatively using exposure times of 4 ms,[3,8] 5 ms,[6,7] 8.4 ms,[3,9] 16 ms,[4] or 20 ms.[5] However, none of the previous clinical studies used exposure times <4 ms, and none have demonstrated the difference in flow sensitivity recorded by multiple exposure times. In this study, we performed MESI intraoperatively during neurosurgery ($n = 8$) with exposure times spanning 0.5 to 20 ms. Images recorded from multiple exposure times were evaluated both individually to emulate single-exposure LSCI and jointly using the MESI model. This article compares the quantitative accuracy and sensitivity of relative flow values computed from MESI and single-exposure LSCI in the human cortex, and demonstrates image calibration and acquisition methods for best performance.

Methods

Instrumentation

A schematic and photograph of the adapted microscope design (Zeiss OPMI Pentero, Carl Zeiss Meditech Inc., Oberkochen, Germany) is shown in Figure 1(a) and (b), respectively. All LSCI hardware components were attached prior to the start of the surgery, and did not interfere with normal use of the microscope during the procedure.

The 785 nm, 300 mW laser diode (LD785–SH300, Thorlabs Inc., Newton, New Jersey, USA) was incorporated into an add-on laser adapter (MM6 Micromanipulator, Carl Zeiss Meditec Inc.) and attached to the bottom of the microscope head. The beam size was $\sim 2 \times 1.5$ cm at a working

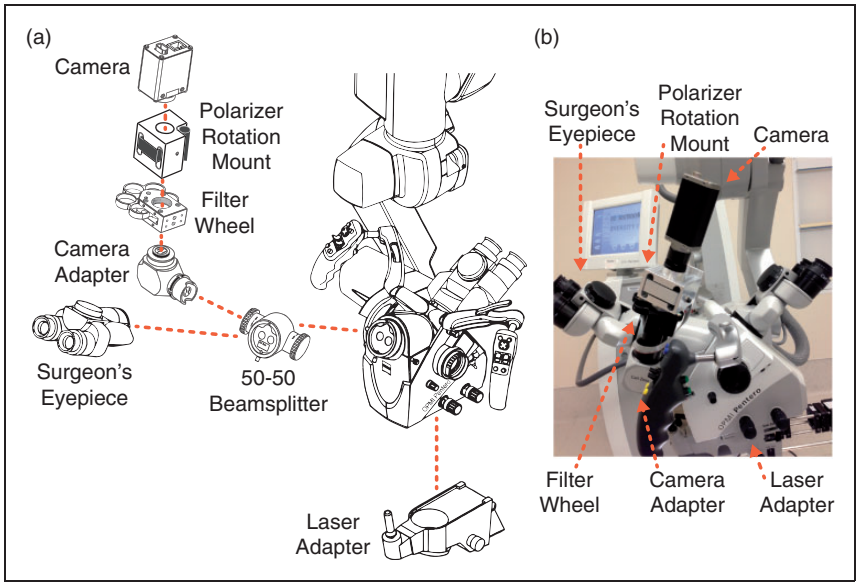

Figure 1. Zeiss OPMI neurosurgical microscope adapted to measure cerebral blood flow intraoperatively using LSCI. (a) Schematic of the intraoperative instrumentation, showing the hardware attachments for LSCI and how they fit into the existing microscope system. Drawings were adapted from the Zeiss OPMI Pentero Manual Issue 9.3. The filter wheel drawing was adapted from Thorlabs Inc. (b) Photograph of the modified intraoperative instrumentation with add-on components labeled.

distance of 30 cm. The maximum irradiance was 0.12 W/cm^2, which is below the ANSI standard of 0.3 W/cm^2 at 785 nm.[12]

The NIR–enhanced CMOS camera sensor (acA1300–60gmNIR, Basler Inc., Ahrensburg, Germany) was recorded using a 905×681 pixel area of interest at an effective frame rate of 75 fps. This resolution was selected to achieve the desired field of view (FOV) matching the laser beam size at the maximum zoom of the microscope. To record the NIR laser light, the LSCI camera was attached to the main surgeon's eyepiece port using a 50–50 beamsplitter and a camera adapter (Carl Zeiss Meditec Inc.). Due to the beamsplitter configuration, the LSCI camera received 12.5% of the total light split within the microscope.

Between the camera and its adapter, the design integrated relay lenses (AC254–060–B, Thorlabs Inc.) to extend the imaging arm for placement of a filter wheel and polarizer rotation mount. The filter wheel (CFW6, Thorlabs Inc.) held various neutral density filters for controlling the laser power in patients 6–8. A polarizer (LPNIR100, Thorlabs Inc.) was integrated into a motorized rotation mount (RSC–100, Pacific Laser Equipment Inc., Santa Ana, California, USA) to reduce specular reflections. A NIR long-pass filter (FF01–715/LP–25, Semrock Inc., Rochester, New York, USA) was added next to the polarizer to allow simultaneous color visualization using the built-in color camera and xenon lamp illumination on the microscope.

Intraoperative procedure

All experiments ($n = 8$) were performed during brain tumor resection procedures at the NeuroTexas Institute at St. David's Medical Center in Austin, TX. The clinical study was approved by the Institutional Review Board of the University of Texas at Austin (#2009-03-0051) and the Austin Multi-Institutional Review Board governing St. David's Medical Center (AMIRB #11-11-01), according to the guidelines in the Belmont Report. Written informed consent was obtained from all patients. LSCI imaging was performed at the discretion of the surgeon, either before or after the tumor resection (see supplemental Table S.1). Prior to LSCI imaging, the surgeon manually positioned the microscope over the cortical area of interest (~30 cm distance), set the microscope for maximum zoom, and focused the microscope. A sterile ruler was used to measure the imaging FOV, since magnification varied slightly between patients. The polarizer was rotated until specular reflections were maximally eliminated in the camera FOV. The surgeon flushed sterile saline over the cortical surface before and during LSCI imaging as needed to reduce specular reflections.

Baseline blood flow image sets of ≤60-s duration were recorded at multiple camera exposure times sequentially. The selection of exposure times was based on the light levels available for each patient, which varied based on the microscope position, the tissue region, and the laser settings. The illumination intensity was matched as closely as possible between camera exposures using the raw image histogram to minimize variations in shot noise. Across all patients, the minimum exposure time was set to either 0.5 or 1 ms to ensure the camera had sufficient light levels at maximum laser power. For patients 1–5, the laser intensity was manually adjusted by lowering the drive current on the laser diode controller to reduce laser power, which required a maximum exposure time of 5 ms to stay above the lasing threshold of the diode. For patients 6–8, the laser intensity was manually adjusted using neutral density filters to maintain more similar laser coherence levels, extending the maximum exposure time to 20 ms. For patient 8, images from five exposure times were acquired before and after minor tissue cautery performed in preparation for the tumor resection. The shortest exposure time available (0.5 ms) was recorded during the tissue cautery (10 s of baseline, followed by 340 s post-cautery).

During the imaging session, the camera exposure signal as well as the patient's electrocardiogram (ECG) and blood pressure (BP) signal were recorded simultaneously (ME590257P, Maguire Enterprises Inc., Fort Lauderdale, Florida, USA). Either the ECG or BP signal was used in post-processing for cardiac cycle sampling and filtering. The total time LSCI added to the surgery was limited to 15 min to minimize additional time under anesthesia, including initial setup of the microscope, imaging, and adjusting laser power between camera exposures.

Image analysis

Speckle image processing. See Supplemental Methods for details on the computation of speckle contrast images. Single-exposure speckle contrast images were computed in real-time using rapid processing techniques[13] integrated into the custom image acquisition software. These images were displayed live on a computer screen during the procedure.

All remaining analysis was performed in post-processing after the surgery. The speckle contrast images were converted to correlation time, τ_c, to provide a more quantitative measure of blood flow.[14] The speckle correlation time τ_c is inversely related to the speed of the moving scatterers,[14,15] and the inverse correlation time ($\mathrm{ICT} = 1/\tau_c$) is commonly used as a metric for blood flow (vasculature) or perfusion (parenchyma).[16,17] In this article, "flow" will be used

throughout for simplicity. See Supplemental Methods for details on the computation of the correlation time for both single-exposure LSCI and MESI analysis.

To improve the accuracy of both single-exposure LSCI and MESI analysis, the instrumentation factor β included in the relationship between speckle contrast and the correlation time was set experimentally for each patient using a simple calibration procedure (see Supplemental Methods, Equations S.2 and S.3). β inherently represents the value of the speckle variance (K^2) when there is no flow, and can be approximated by K^2 for that particular imaging configuration as the exposure time goes to zero ($\lim_{T\to 0} K^2 = \beta + v_{noise} \sim \beta$). Thus, a static sample was imaged at the shortest exposure time available and the average speckle variance (K^2) from this region was used to estimate β. This static calibration procedure accounted for variations in β on a case-by-case basis, including the no-flow speckle variance for each tissue region, the angle of illumination, and the magnification. A sterile ruler placed on the cortical surface served as the static sample region for case 3 (Figure 2(a)), case 7 (Figure 2(b)), and case 8 (Figure 2(c)), which are shown as the magenta ROIs ($\beta = 0.19$, 0.15, and 0.21, respectively).

See Supplemental Methods for details regarding additional image processing, including image registration, cardiac cycle sampling, and cardiac filtering. In summary, speckle contrast images across all exposure times were aligned to a single frame from a single exposure time using automatic intensity-based image registration with *Elastix*,[18] similar to previous work.[7] Registered images were selected from the same 0.2-s normalized time window of the cardiac cycle to synchronize with the heartbeat and minimize pulsatile variation across exposure times.[6,7,19] Fifty images spanning multiple heartbeats were averaged for each exposure time to reduce noise for the computation of MESI ICT maps. A sub-set of recorded images (20–30 s, 1400–2000 frames) from each exposure time was used for analysis on select regions of interest (ROIs), which were cardiac filtered similar to previous work.[6,7,19] ICT values were computed and displayed as summary values, since each exposure corresponded to different time points. For the single-exposure LSCI recording during tissue cautery in case 8, ROI data were cardiac filtered, smoothed using a 0.5-s moving average filter, and displayed as a time course.

Speckle validation—Conservation of flow analysis. To validate the quantitative accuracy of the MESI model in clinically acquired data, select ROIs were chosen that spanned a vessel bifurcation, including one parent and two daughter vessels. Then, assuming normal physiological conditions, flow conservation analysis was performed to determine how well the single-exposure LSCI and MESI flow estimates agreed with conserved flow at each vessel branch. This analysis method has previously been demonstrated,[20] and serves as a useful validation of the accuracy of speckle-computed flows. For this vascular analysis, ICT was linearly scaled by the vessel diameter (D) to account for differences in tissue volume sampling over vessels of various calibers.[21]

The MESI ICT frames were used to estimate the vessel diameters of interest. The midline of the vessel was manually drawn along the length of the ROI, and equally spaced perpendicular profiles were automatically selected. The first derivative (slope) of each profile was computed to define the edge of the vessel, and the average diameter along the length of the ROI was used to define D. To avoid speckle-related bias in the blood flow metric (ICT·D), parent vessel identification was performed based on the vessel diameter. Within each

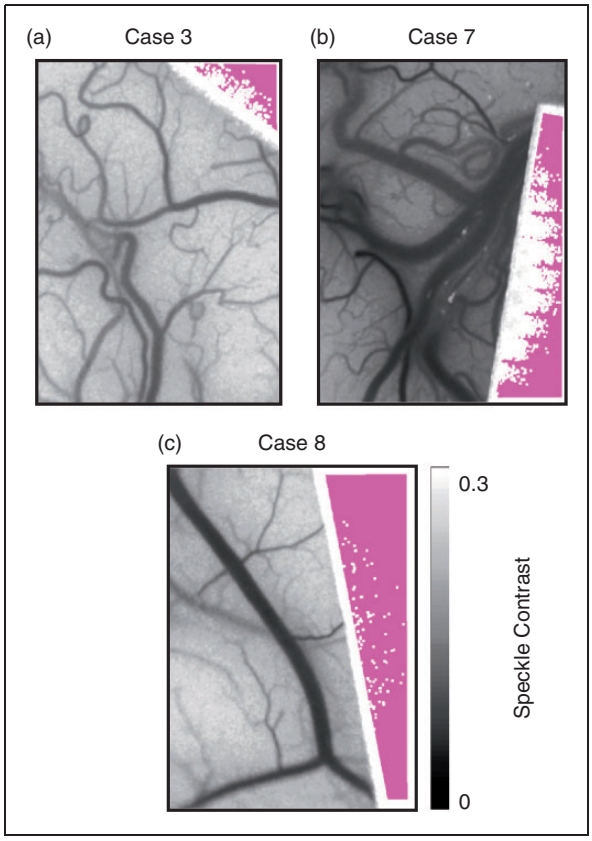

Figure 2. The static regions selected for the calculation of β are shown as the magenta ROIs overlaid on the gray scale speckle contrast images for case 3 (a), case 7 (b), and case 8 (c). The color bar applies to all frames, where black indicates faster flow. The shortest exposure time image from each case (0.5 ms) was used for this calibration procedure. The static reference was a sterile ruler for all cases, and $\beta = 0.19$, 0.15, and 0.21, respectively.

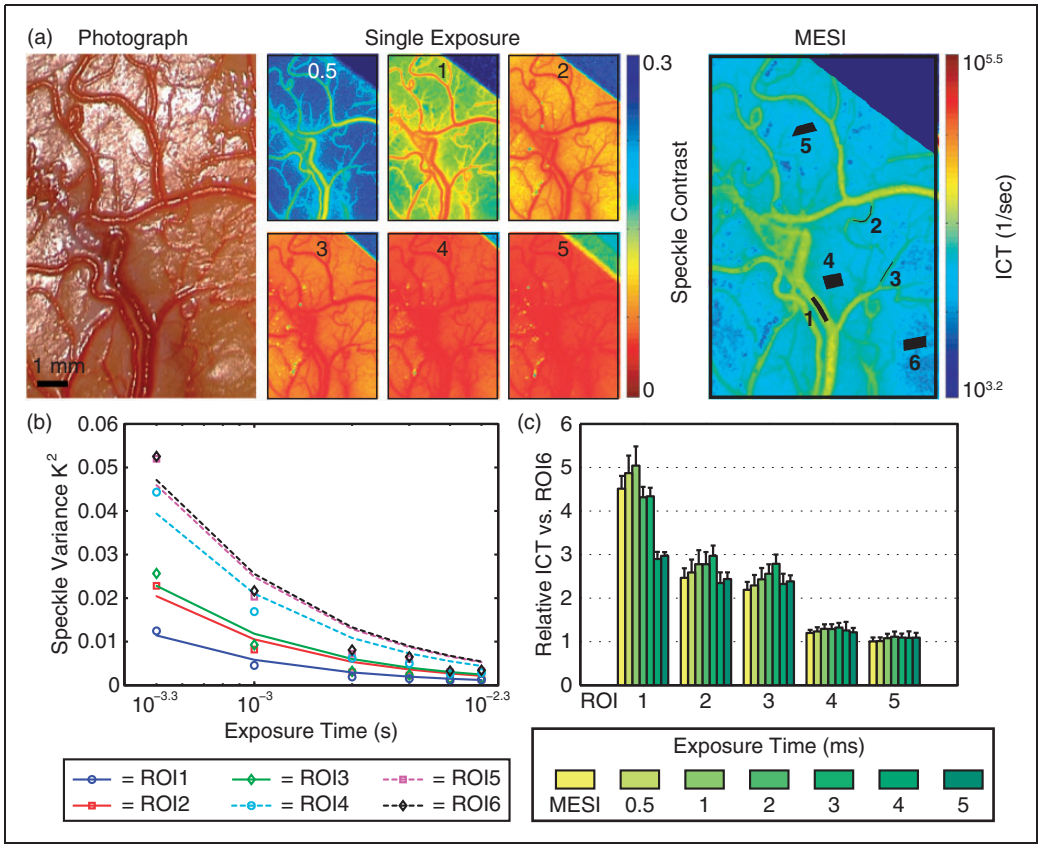

Figure 3. (a) Color photograph (left), six single-exposure LSCI frames spanning 0.5–5 ms (middle), and the corresponding MESI ICT map (right) from patient 3. Scale bar (black) = 1 mm. The color bar for the single-exposure LSCI images applies to all six frames, and the color bar on the right applies to the MESI frame. Lower speckle contrast and higher ICT values (both red) indicate faster flow. The numbered ROIs used for analysis are shown in black in the MESI ICT frame. (b) MESI-computed speckle visibility curves for each of the six ROIs shown on a semi-logarithmic scale. The median fits are given by the solid or dotted lines, and the points show the median of the measured data. (c) Relative ICT comparison across ROIs (average ± standard deviation) using ROI6 as a baseline (slowest flow), computed for the MESI model (M) as well as each of the individual exposure times measured.

branch, the largest computed diameter was assumed to be the parent vessel (p), and the two remaining branches were assumed to be the daughter vessels (1, 2). Then, the percent error was calculated assuming conservation of flow, given by

$$\%\text{Error} = \frac{\left|D_1/\tau_{c1} + D_2/\tau_{c2} - D_p/\tau_{cp}\right|}{D_p/\tau_{cp}} \times 100 \qquad (1)$$

Results

Single-exposure LSCI images are displayed as speckle contrast images, since they represent an instantaneous qualitative 2D map of blood flow. All single-exposure LSCI frames are equally scaled from 0 to 0.3 (speckle contrast) to span the full range of the speckle contrast histogram across all patients, but images cannot be quantitatively compared across patients. The MESI ICT frame combines information from all exposures, which displays a more quantitative map of blood flow than any single exposure time alone.[10] All MESI ICT frames are equally scaled from $10^{3.2}$ to $10^{5.5}$ (ICT, 1/s) to span the full range of the ICT histogram across all patients, which allows easy inter-patient comparisons. Supplemental Figure S.1 (single-exposure LSCI frames from cases 2 and 5), Figure S.2 (spatial R^2 maps for MESI ICT frames), and Table S.2 (quantitative overview of MESI goodness-of-fit) are provided for reference.

MESI model vs. single-exposure LSCI: Sensitivity

This section highlights quantitative flow analysis of ROIs spanning vessel and parenchyma regions using both the single-exposure LSCI and MESI models. The main goal was to assess how well the MESI model matched measured results and whether the results followed expected physiological trends. Cases 3 (Figure 3) and 7 (Figure 4) are highlighted for baseline

flow assessment. The speckle variance K^2 is plotted against the exposure time T on a semi-logarithmic scale to visualize goodness-of-fit of the experimental data with the MESI model, which is known as the speckle visibility curve.[11] A spatial relative ICT comparison was also performed using the slowest flowing ROI6 as the baseline for comparison between single-exposure and MESI estimates. This spatial normalization was used to highlight the sensitivity differences between the MESI model and the individual exposure times.

The color photograph, single-exposure images, and MESI ICT frame for case 3 are shown in Figure 3(a). This cortical tissue region has relatively small vascular caliber, with all vessels <470 µm diameter. The shortest exposure time (0.5 ms, max $K = 0.29$) provides the best visibility among larger diameter vasculature, while smaller cortical vessels are more easily visualized in the 1 and 2 ms images (max $K = 0.18$ and 0.12, respectively). The MESI ICT frame shows relatively slow flows spanning only a portion of the full ICT range visualized.

Three vessel ROIs and three parenchyma ROIs were selected, spanning various vessel sizes and spatially sampling different tissue regions. The speckle visibility curves for each ROI are shown in Figure 3(b), highlighting that these exposure times sample the upper tail end of the sigmoidal speckle visibility curve. These curves show the expected trend physiologically between the different ROI regions selected. For the three vessel regions, the decays proceed in the expected order by vessel size, with the largest vessel having the fastest decay and the smallest vessel with the slowest decay. All parenchymal regions have slower decays than the vessel regions, and the flow order follows the color map seen in both the single-exposure and MESI frames. From these curves, all ROIs fit the average across exposure times ($R^2 = 0.94 \pm 0.02$, 12,000 fits).

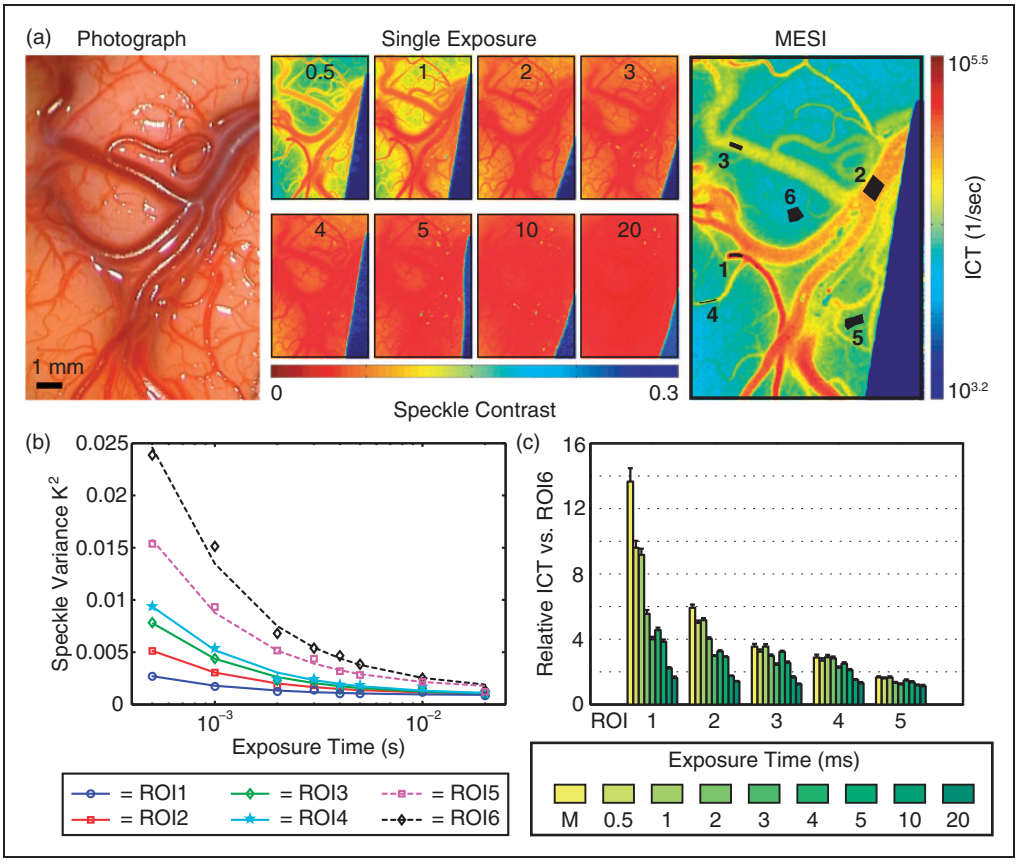

Figure 4. (a) Color photograph (left), eight single-exposure LSCI frames spanning 0.5–20 ms (middle), and the corresponding MESI ICT map (right) from patient 7. Scale bar (black) = 1 mm. The color bar for the single-exposure LSCI images applies to all eight frames, and the color bar on the right applies to the MESI frame. Lower speckle contrast and higher ICT values (both red) indicate faster flow. The numbered ROIs used for analysis are shown in black in the MESI ICT frame. (b) MESI-computed speckle visibility curves for each of the six ROIs shown on a semi-logarithmic scale. The median fits are given by the solid or dotted lines, and the points show the median of the measured data. (c) Relative ICT comparison across ROIs (average ± standard deviation) using ROI6 as a baseline (slowest flow), computed for the MESI model (M) as well as each of the individual exposure times measured.

For the spatial relative ICT comparison in Figure 3(c), the estimated flow distributions from MESI and the individual exposure times highlight that each model provides a different estimate of the relative flows across the FOV. Each ROI has a different exposure that provides the broadest relative flow distribution indicating the maximal sensitivity (1, 2, or 3 ms). The MESI results fit the average between the low and high exposures and most closely match 0.5, 3, or 5 ms, depending on the ROI.

The color photograph, single-exposure images, and MESI ICT frame for case 7 are shown in Figure 4(a). This cortical tissue region has four large diameter vessels (~0.5–1 mm) in the right central portion of the FOV. The shortest exposure time (0.5 ms, max $K = 0.20$) again provides high differentiation between the flows within the large vessel branches, and clearly shows that a ~0.25 mm diameter arteriole has the fastest flow in the FOV. This would not be expected from the vessel diameter alone, but is clinically feasible if the larger vessel branches are slow flowing draining veins. For the longer exposure times, sensitivity to differences between vascular flows decreases (10–20 ms), and vascular and parenchymal flows become more similar (20 ms). Here, the MESI ICT map shows faster flows compared to case 3 in the large vessel branches and in the small diameter arteriole.

Select ROIs were chosen spanning four vessels and two parenchyma regions, shown on the MESI ICT frame in Figure 4(a). The speckle visibility curve in Figure 4(b) shows excellent fits across almost all exposure times and all ROIs ($R^2 = 0.98 \pm 0.01$, 8400 fits). This case also has excellent fits across the entire FOV ($R^2 = 0.98 \pm 0.03, > 3.97 \times 10^5$ fits, see supplemental file). The small diameter arteriole ROI1 has the fastest decay, followed by the large vessels ROIs 2 and 3, and finally the small cortical vessel ROI4. The parenchyma ROIs follow with slower decays in the order expected from both the MESI and single-exposure images.

For the spatial relative ICT comparison in Figure 4(c), the MESI-computed relative flows have the broadest flow distribution across all ROIs. The MESI flow prediction for arteriole ROI1 (13.6×) has >40% larger magnitude compared to the next closest single-exposure times (9.6× and 9.2× for 0.5 and 1 ms, respectively). Flow predictions continue to decrease as exposure times increases (2–10 ms, 5.6× → 2.2× for ROI1), with similar trends observed across all ROIs. The longest exposure time (20 ms) shows very little differentiation among vastly different tissue ROIs (1.1× to 1.6×). Due to the faster flows in this case, the MESI results most closely match the 0.5 or 1 ms exposure time, depending on the ROI.

MESI model vs. single-exposure LSCI: Accuracy

Next, conservation of flow analysis was performed to further validate the quantitative accuracy of the MESI model in comparison to the single-exposure LSCI estimates. The ROIs used to compute the ICT values are shown in different colors for each bifurcation. Results are illustrated for cases 3 (Figure 5(a)) and 7 (Figure 5(b)) in four Y-branches each, with the MESI percent error for each branch indicated in the

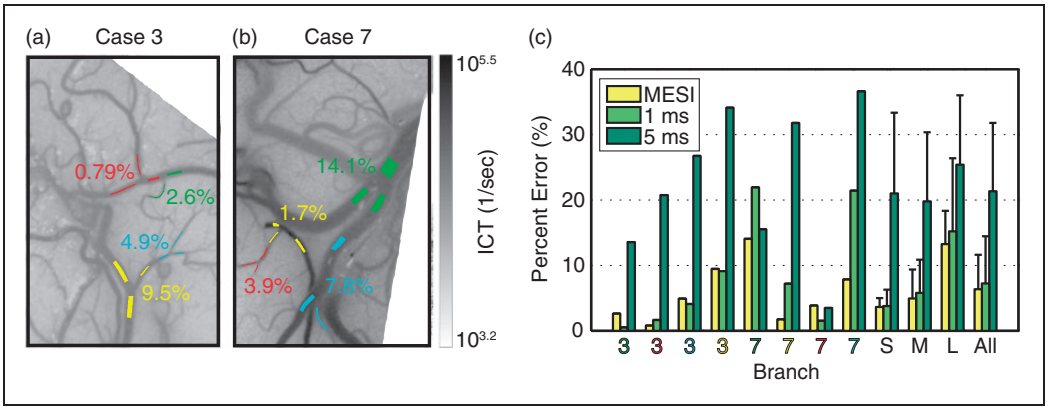

Figure 5. Conservation of flow analysis for three-way vessel branches, shown for case 3 (a) and case 7 (b) in four branches each. All grouped vessel branches are shown in the same color, overlaid on the gray scale MESI ICT map. The MESI-computed percent error between the addition of flows from the two daughter vessels and the flow from the parent vessel is shown for each branch in its associated color. (c) The percent error (%) using ICT values computed from MESI (yellow), as well as from 1 ms (light green) and 5 ms (dark green) single-exposure LSCI. Each individual branch from (a) and (b) is highlighted, as well as the average and standard deviation across five cases for small (S) branches (<200 μm, $n = 4$), medium (M) branches (200–500 μm, $n = 7$), large (L) branches (>500 μm, $n = 3$), and all branches ($n = 14$).

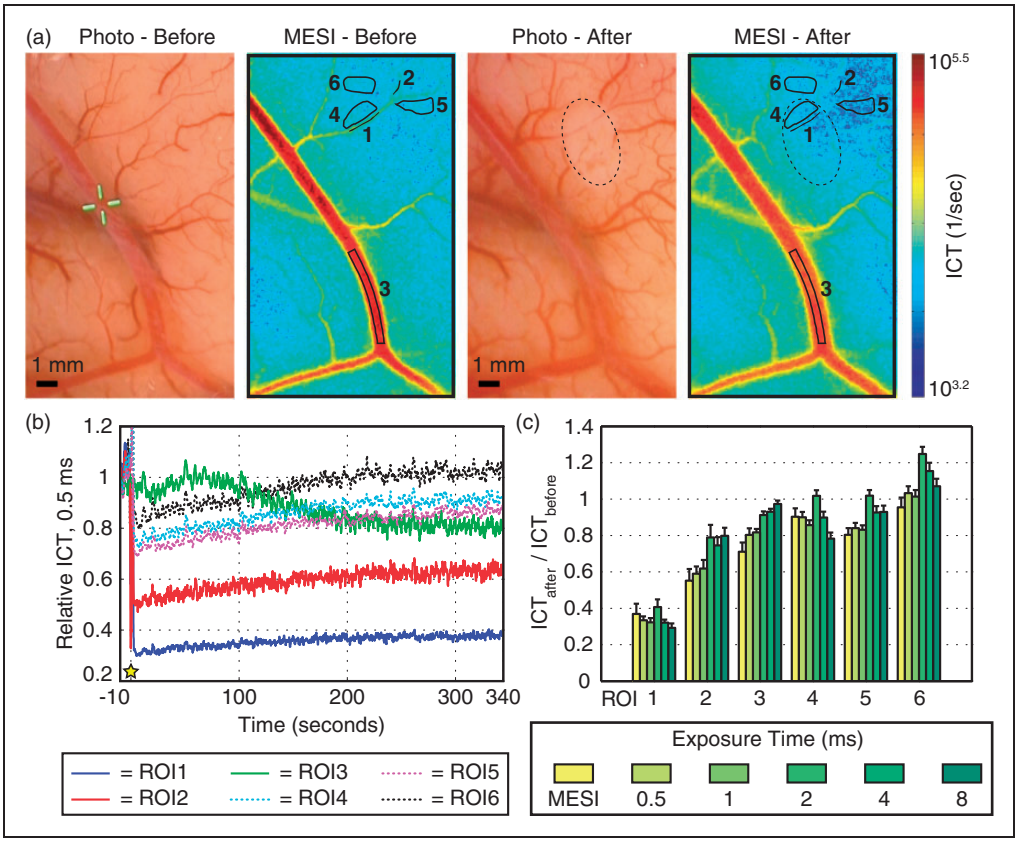

Figure 6. (a) Color photographs and corresponding MESI ICT maps computed from five single-exposure LSCI sets (0.5–8 ms) before (left) and after (right) tissue cautery in patient 8. Scale bar (black) = 1 mm. The black dotted line indicates the region where minor bipolar cautery took place. The color bar on the right applies to both MESI frames, where higher ICT values (red) indicate faster flow. The numbered ROIs used for analysis are shown with a black outline in the MESI ICT frame. (b) Relative ICT time course computed from the 0.5 ms LSCI recording before, during, and after the tissue cautery. This recording includes 10 s of baseline, cautery at time 0 indicated by the yellow star, and 340 s post-cautery. Each region was normalized to its own respective baseline ICT value before the cautery. (c) Relative ICT comparison across ROIs (average ± standard deviation) computed for the MESI model as well as each of the individual exposure times measured. The relative ICT values display the relative change in flow due to cautery, given by ICT_{after} normalized by ICT_{before}.

same color. A comparison between the MESI estimate versus two single exposure times, 1 and 5 ms, is shown in Figure 5(c). This includes each individual Y-branch shown in Figure 5(a) and (b), as well as an overview across five total cases split into small branches (<200 µm, $n = 4$), medium branches (200–500 µm, $n = 7$), large branches (>500 µm, $n = 3$), and all branches ($n = 14$). Across cases 3 and 7, all MESI-computed percent errors are <10%, with the exception of the large vessel branch (green) in case 7. Overall, the MESI computation produced the lowest percent error at 6.4% ± 5.3%, followed closely by the 1-ms exposure time 7.2% ± 7.2%, and finally the 5 ms exposure time at 21% ± 10%. Grouped by vessel size, the smallest branches had the lowest error in the MESI estimates (3.7% ± 1.4%), followed by the medium branches (5.0% ± 4.4%), and the largest vessel branches (13% ± 5.1%).

MESI model application: Before and after tissue cautery

Finally, MESI was performed before and after tissue cautery in case 8 to demonstrate the clinical utility of using MESI versus single-exposure LSCI to monitor blood flow changes during the surgery. Figure 6(a) shows color photographs and MESI ICT frames recorded before and after the tissue cautery. The MESI frame was computed from five single-exposure LSCI sets (0.5–8 ms), and displays six ROIs spanning both vessel and parenchyma regions affected by the tissue cautery. The six ROIs had good MESI fitting performance, with goodness-of-fit values in between the two previously presented cases ($R^2 = 0.96 \pm 0.02$ before cautery, $R^2 = 0.98 \pm 0.02$ after cautery, 8400 fits). The post-cautery ICT image showed reduced flow in the location where cautery took place, in the upper right quadrant

near ROIs 2 and 5, and in the large central vessel (ROI3) accompanied by vessel dilation. Figure 6(b) shows the relative ICT time course for the 0.5 ms LSCI recording before, during, and after the tissue cautery, where each region has been normalized to its respective baseline ICT values before the cautery. Here, ROIs 1, 2, 4, and 5 show a decrease in flow followed by partial recovery, ROI6 shows a decrease in flow followed by a full recovery, and ROI3 shows a decrease in flow starting at ~100 s. Figure 6(c) shows a relative ICT comparison between MESI and single-exposure values after tissue cautery, where each ROI is normalized to the ICT value before tissue cautery to highlight the flow change. ROIs 2, 3, 5, and 6 have the largest flow reduction in the MESI estimate with generally increasing reduction estimates as exposure time increases, while ROIs 1 and 4 closest to the occlusion location show the opposite trend.

Discussion

MESI model implementation in a clinical setting

The results of the MESI model implementation in the clinic demonstrate that proper image acquisition and processing of clinical MESI images can result in excellent fitting performance (case 7) and clinically reasonable flow estimates. This study used multiple techniques to improve the fitting accuracy at the upper and lower exposure time limits, and to overcome the limited exposure time range available (0.5–20 ms). The first component that led to high goodness-of-fit was modifying the laser power using neutral density filters. This stabilized laser coherence across exposures and enabled acquisition of longer exposure times, which helped improve fitting accuracy approaching the upper exposure time limit. The second component that led to clinically feasible flow rates was the calibration procedure used to set the instrumentation factor, β, for every patient. Fixing β using a static reference reduced the search space of the nonlinear fit,[11,22] which improved fitting accuracy and produced realistic flow trends that made sense physiologically across all cases. Unavoidable tissue motion prevents even the sterile ruler from being a fully static sample, confirmed by the speckle variance decay with increasing exposure time. However, the calibration procedure uses only the shortest exposure time to estimate the no-flow speckle variance, which minimizes integration of tissue motion. Because β is an estimate for the lower limit of the speckle variance at very short exposure times, this calibration helped the MESI model fit the full speckle visibility curve from the small range of measurable exposure times.[22] In addition, β is a shared variable in both single-exposure and MESI models (supplemental Equations S.2 and S.3), meaning that reliable estimates of β can also be used for the computation of single-exposure ICT values. Integrating β estimates in the single-exposure model provided excellent agreement with the MESI model for the shorter exposure times, indicating that this simple calibration procedure during image acquisition can be used to improve accuracy even in single-exposure LSCI. Both of these procedures contributed to accurate nonlinear curve fitting of the MESI model, produced reliable computation of quantitative flow information for each patient, and accounted for instrument variations from case-to-case.

Comparing MESI vs. single-exposure LSCI performance

The results from this study demonstrate differences in relative flow sensitivity measured from MESI versus single-exposure LSCI in the human brain. Each exposure time is sensitive to a different range of flows,[22] and the shorter exposure times provided the best flow sampling for the larger caliber vasculature seen in the human cortex. The maximum sensitivity (broadest relative flow distribution) depended on the magnitude of flow in the cortical region. The smaller caliber vasculature region (case 3) maximized across several mid-range exposure times (1–3 ms), while the larger caliber vasculature region (case 7) maximized with the MESI estimates followed by the shortest exposures (0.5–1 ms). The shorter exposure times in previous intraoperative LSCI studies (4–5 ms)[3,6–8] are comparable to the optimal sensitivity for the rodent cortex,[23] but the caliber of human cortical vasculature is much larger and their associated flow rates are much faster. The longest exposure times in previous studies (8.4–20 ms)[3–5,9] are comparable to the longer exposures measured in case 7, which had poor sensitivity among different tissue regions (<2.2× relative flow span). This is likely due to improper matching of the exposure time with the flows sampled and increasing integration of tissue motion artifacts within the camera exposure time, which results in faster speckle de-correlation. Some of the previous studies may have selected a longer exposure time to focus on blood flow in parenchyma tissue regions,[5,9] while others may have been simply light limited.[4] Similar to previous animal studies,[10] there is not a single exposure time that has optimal sensitivity for the full range of flows measurable in a clinical setting, and MESI will always provide a broader and more reliable sampling of the flow distribution.

The conservation of flow analysis revealed that both MESI and 1 ms LSCI provided excellent estimates for physiologically accurate flows in vessel bifurcations (<10%). The 5 ms exposure time had a larger error

(>20%), suggesting that this exposure time was less sensitive to the flow range measured in the human cortex. Although this analysis does not confirm absolute flow accuracy, it does provide an indicator for how accurately the measured flow distribution matches expected physiology in the absence of an alternate measurement technique. These results are consistent with previous work in rodent vasculature[21] and retinal vasculature[20] with vessel diameters <200 μm. These studies showed a strong correlation between a diameter-scaled LSCI flow metric and absolute flows[21] or conserved vascular flows,[20] respectively. Grouped by vessel size, the smallest branches (<200 μm) had the lowest error followed by the medium branches, with comparable errors across MESI and 1 ms LSCI. The highest error (>10%) was from the largest vessel branches (>0.5 mm), which could indicate that the diameter-scaled flow metric breaks down in larger diameter vasculature. Speckle imaging of a vessel region samples dynamically scattered light that is spatially localized to the vascular region.[24] As vessel size increases, only the top fraction of the full cross-sectional area will be sampled. The diameter scaling may then overestimate the number of dynamic scattering events for that vessel, and increase errors in the computed conservation of flow. In addition, the shortest exposure time used in this study (0.5 ms) may not be short enough to properly sample the flow rates in large diameter vessels. Improper sampling of the flow, even with MESI, could lead to higher error in the computed ICT values. High error (>10%) in conservation of flow analysis could serve as an indicator for inaccurate blood flow estimates (ICT·D).

Imaging before and after minor tissue cautery demonstrated that MESI was able to detect small changes in regional blood flow in areas adjacent to the surgical field. The MESI ICT images spatially highlight the region with reduced flow, while the single-exposure LSCI time course highlights the real-time blood flow dynamics after tissue cautery. The spatial relative ICT analysis demonstrated that four of six ROIs had greater flow reduction measured by MESI than any of the single-exposure LSCI estimates. This is consistent with previous animal occlusion studies, where MESI estimates depicted greater ischemia than single-exposure LSCI and were shown to have higher accuracy compared to absolute speeds.[10] ROIs 1 and 4 closest to the occlusion showed the opposite trend, which could be due to continuing flow changes in these regions. The post-cautery single-exposure LSCI frames were recorded immediately after the time course, and flow had not returned completely to steady state (only ROI6 returned to baseline). This may also explain why the 2 ms relative ICT estimates are higher than the other single-exposure estimates. This example highlights the practical applicability of MESI for quantitative intraoperative blood flow monitoring.

Why MESI vs. single-exposure LSCI?

Overall, the results from this study demonstrate that MESI and short single-exposure LSCI flow estimates (0.5–1 ms) provide similar sensitivity and comparable quantitative accuracy. This similarity could be due to multiple factors, including identical experimental conditions, absence of static scatterers, and estimation of β. In the absence of static scatterers ($\rho = 1$), the MESI speckle visibility expression (supplemental Equation S.3) simplifies to the single-exposure model (supplemental Equation S.2), with the addition of a noise term. Given that the dura mater was removed prior to speckle imaging, it is reasonable that the presence of static scatterers should be limited ($\rho \to 1$). In addition, the calibration procedure produced an estimate of the instrumentation factor β that could be used for both MESI and single-exposure flow estimates. This article demonstrates examples where short single-exposure LSCI performs comparably to MESI under the same illumination conditions, without static scattering ($\rho \to 1$), and with an estimate for β. Under these conditions, the single-exposure speckle model should produce the same τ_c estimates as the MESI model, with an appropriate exposure time selection maximizing speckle sensitivity ($T \sim \tau_c$).[22]

Despite this similarity, the MESI ICT computations are less susceptible to variations in experimental conditions and are more reliable compared to single-exposure LSCI.[11] There are scenarios when LSCI will be less accurate than MESI, such as in the presence of static scattering.[11,25] In addition, LSCI cannot account for the shape of the speckle visibility curve, and requires careful selection of the camera exposure time to maximize sensitivity.[22] This optimal exposure time depends on the vessel size and flow magnitude in the cortical region and is difficult to predict in advance. Thus, it is risky to rely on single-exposure LSCI for quantitative flow estimates, and these measurements are limited to qualitative visualization.

MESI provides a more reliable quantitative baseline and allows inter-patient comparisons,[10,21,26] which is a critical advantage compared to single-exposure LSCI for intraoperative applicability. The equally scaled ICT frames (Figures 3, 4, and 6) show similar parenchymal flows with a broad range of vascular flows. Figure 3 shows the slowest vascular flows consistent with the smallest vessel caliber, Figure 6 shows the fastest vascular flow consistent with large arterial flow, and Figure 4 shows large draining veins flowing slower than a small diameter arteriole. Vessel

classifications were inferred based on surgeon input from the color photographs and the inherent flow differences in the ICT maps. The physical appropriateness of blood flow estimates is an important indicator of the reliability of the MESI model results, and should be verified by the user. Overall, the MESI model produced clinically valid flow estimates, with physiologically feasible relationships between vessels based on caliber or type.

Limitations and future directions

This intraoperative MESI study had some inherent limitations associated with the instrument design and image processing. The instrument design required exposure times to be acquired sequentially, rather than interleaved as is common in laboratory MESI systems.[10,11] Thus, the time span between the first and last recorded image in a given case was typically >10 min, yet the image analysis procedure assumes physiological uniformity across exposure times. Cardiac filtering for ROI analysis and restricting image selection to the same region of the cardiac cycle for MESI ICT image generation should minimize the effects of heart rate and blood flow variation, but cannot eliminate them completely. In addition, this long recording time span led to differences in cortical surface hydration across exposure times, resulting in increased specular reflections at longer intervals from saline application. Future work should include interleaved MESI acquisition using an optical modulator similar to laboratory setups to reduce the error resulting from changing physiology and tissue hydration during the imaging session.

The lower limit for the exposure time in this study was 0.5 ms; however, even shorter exposure times are required to capture the full speckle visibility range for human cortical tissues.[22] For cases 3 and 7, theoretical estimates indicate that the speckle visibility approaches the respective β value at exposure times that are three to four orders of magnitude shorter than what was measured in this study (see supplemental Figure S.3). Future work should include recording at shorter exposure times to determine the required exposure time range to visualize human cortical blood flow magnitudes.

Because all images had to be aligned before MESI analysis, all quantitative image processing was completed after the completion of the case. Real-time implementation of image registration, cardiac filtering, and MESI fitting using parallel processing methods is critical to move MESI towards future clinical use as an intraoperative monitoring system. In addition, scaling vascular MESI ICT estimates by real-time diameter measurements (ICT·D) intraoperatively would provide a more quantitatively accurate flow distribution.

The MESI ICT frames are currently displayed with an arbitrary logarithmic scale (1/s), which is difficult to relate to absolute blood flow or perfusion.[27–29] However, this scale is quantitative and can be compared across patients, meaning that a fixed display range could be clinically useful even though the units are not absolute. In addition, future integration with neurosurgical microscopes could allow real-time visualization of MESI frames in the surgeon eyepiece. The MESI frame could be superimposed on the color photograph to show relative changes in tissue perfusion during the procedure, providing the surgeon with a tool to directly visualize the impact of each intervention and tailor the approach with real-time data. In addition, quantitative thresholds could be defined to highlight under-perfused regions in danger of tissue death. MESI has the potential to be clinically useful for monitoring distal brain regions during vascular procedures or in regions of elevated pressure.

Future studies should record physiological parameters important for cortical blood flow, including mean arterial blood pressure (MAP) and the arterial partial pressure of carbon dioxide ($PaCO_2$). Matching these parameters across patients would allow a more controlled physiological study to compare MESI ICT results across a wider range of cortical regions and neurosurgical applications. Future studies should also include a larger patient cohort to determine the true MESI ICT clinical range for scaling images, to further validate MESI accuracy (conservation of flow) and sensitivity to flow changes, and to develop quantitative thresholds for surgical decision-making.

Conclusions

The results from this clinical study demonstrate that intraoperative MESI maximizes the sensitivity and physiological accuracy of blood flow estimates. Comparable performance was obtained by short single-exposure LSCI ($\leq$1 ms), but this remains a less reliable approach limited to qualitative assessment. Estimating the instrumentation factor β and using neutral density filters to control the laser power provided excellent MESI fitting performance, confirming robust MESI model implementation in a clinical setting. Clinical MESI has high potential for quantitative intraoperative CBF monitoring, and future clinical studies are warranted across a broader range of neurosurgical procedures.

Funding

The author(s) disclosed receipt of the following financial support for the research, authorship, and/or publication of this article: This work was funded by grants from The Coulter Foundation, the National Institutes of Health (EB011556,

NS078791, NS082518, EB007507), and the American Heart Association (14EIA8970041).

Acknowledgments

The authors would like to acknowledge the research and surgical staff at St. David's Medical Center, especially Sergio Avila-Michel, for their help with the experiments.

Declaration of conflicting interests

The author(s) declared no potential conflicts of interest with respect to the research, authorship, and/or publication of this article.

Authors' contributions

LMR and KEO built the clinical imaging system. LMR, SMSK, JSW, and DJF acquired the data. LMR and SMSK analyzed the results. DJF and AKD conceived the project. AKD supervised the project. LMR wrote the manuscript. All authors contributed to manuscript revisions.

Supplementary material

Supplementary material for this paper can be found at http://journals.sagepub.com/doi/suppl/10.1177/0271678X16686987

References

1. Kirkness CJ. Cerebral blood flow monitoring in clinical practice. *AACN Clin Issues* 2005; 16: 476–487.
2. Hecht N, Woitzik J, Dreier JP, et al. Intraoperative monitoring of cerebral blood flow by laser speckle contrast analysis. *Neurosurg Focus* 2009; 27: E11.
3. Hecht N, Woitzik J, Konig S, et al. Laser speckle imaging allows real-time intraoperative blood flow assessment during neurosurgical procedures. *J Cerebr Blood Flow Metab* 2013; 33: 1000–1007.
4. Nomura S, Inoue T, Ishihara H, et al. Reliability of laser speckle flow imaging for intraoperative monitoring of cerebral blood flow during cerebrovascular surgery: comparison with cerebral blood flow measurement by single photon emission computed tomography. *World Neurosurg* 2014; 82: e753–e757.
5. Klijn E, Hulscher HC, Balvers RK, et al. Laser speckle imaging identification of increases in cortical microcirculatory blood flow induced by motor activity during awake craniotomy. *J Neurosurg* 2013; 118: 280–286.
6. Parthasarathy AB, Weber EL, Richards LM, et al. Laser speckle contrast imaging of cerebral blood flow in humans during neurosurgery: a pilot clinical study. *J Biomed Opt* 2010; 15: 066030.
7. Richards LM, Towle EL, Fox DJ Jr, et al. Intraoperative laser speckle contrast imaging with retrospective motion correction for quantitative assessment of cerebral blood flow. *Neurophotonics* 2014; 1: 015006.
8. Woitzik J, Hecht N, Pinczolits A, et al. Propagation of cortical spreading depolarization in the human cortex after malignant stroke. *Neurology* 2013; 80: 1095–1102.
9. Hecht N, Müller M-M, Sandow N, et al. Infarct prediction by intraoperative laser speckle imaging in patients with malignant hemispheric stroke. *J Cerebr Blood Flow Metab* 2016; 36: 1022–1032.
10. Kazmi SMS, Parthasarathy AB, Song NE, et al. Chronic imaging of cortical blood flow using Multi-Exposure Speckle Imaging. *J Cerebr Blood Flow Metab* 2013; 33: 798–808.
11. Parthasarathy AB, Tom WJ, Gopal A, et al. Robust flow measurement with multi-exposure speckle imaging. *Opt Express* 2008; 16: 1975–1989.
12. American National Standard for the Safe Use of Lasers. *ANSI Z1361-2007*. Orlando, FL: Laser Institute of America, 2007.
13. Tom WJ, Ponticorvo A and Dunn AK. Efficient processing of laser speckle contrast images. *IEEE Trans Med Imag* 2008; 27: 1728–1738.
14. Briers JD and Webster S. Laser speckle contrast analysis (LASCA): a nonscanning, full-field technique for monitoring capillary blood flow. *J Biomed Opt* 1996; 1: 174–179.
15. Bonner R and Nossal R. Model for laser Doppler measurements of blood flow in tissue. *Appl Opt* 1981; 20: 2097–2107.
16. Ayata C, Dunn AK, Gursoy-Özdemir Y, et al. Laser speckle flowmetry for the study of cerebrovascular physiology in normal and ischemic mouse cortex. *J Cerebr Blood Flow Metab* 2004; 24: 744–755.
17. Strong AJ, Bezzina EL, Anderson PJB, et al. Evaluation of laser speckle flowmetry for imaging cortical perfusion in experimental stroke studies: quantitation of perfusion and detection of peri-infarct depolarisations. *J Cerebr Blood Flow Metab* 2005; 26: 645–653.
18. Klein S, Staring M, Murphy K, et al. elastix: a toolbox for intensity-based medical image registration. *IEEE Trans Med Imaging* 2010; 29: 196–205.
19. Richards LM, Towle EL, Fox DJ, et al. Laser speckle imaging of cerebral blood flow. In: Madsen SJ (ed.). *Optical methods and instrumentation in brain imaging and therapy*. New York: Springer, 2013, pp.117–136.
20. Shiga Y, Asano T, Kunikata H, et al. Relative flow volume, a novel blood flow index in the human retina derived from laser speckle flowgraphy. *Invest Ophthalmol Vis Sci* 2014; 55: 3899–3904.
21. Kazmi SMS, Faraji E, Davis MA, et al. Flux or speed? Examining speckle contrast imaging of vascular flows. *Biomed Opt Express* 2015; 6: 2588–2608.
22. Kazmi SMS, Balial S and Dunn AK. Optimization of camera exposure durations for multi-exposure speckle imaging of the microcirculation. *Biomed Opt Express* 2014; 5: 2157–2171.
23. Yuan S, Devor A, Boas DA, et al. Determination of optimal exposure time for imaging of blood flow changes with laser speckle contrast imaging. *Appl Opt* 2005; 44: 1823–1830.
24. Davis MA, Kazmi SMS and Dunn AK. Imaging depth and multiple scattering in laser speckle contrast imaging. *J Biomed Opt* 2014; 19: 086001.

25. Parthasarathy AB, Kazmi SMS and Dunn AK. Quantitative imaging of ischemic stroke through thinned skull in mice with Multi Exposure Speckle Imaging. *Biomed Opt Express* 2010; 1: 246–259.
26. Kazmi SMS, Wu RK and Dunn AK. Evaluating multi-exposure speckle imaging estimates of absolute autocorrelation times. *Opt Lett* 2015; 40: 3643–3646.
27. Duncan DD and Kirkpatrick SJ. Can laser speckle flowmetry be made a quantitative tool? *J Opt Soc Am A* 2008; 25: 2088–2094.
28. Briers D, Duncan DD, Hirst E, et al. Laser speckle contrast imaging: theoretical and practical limitations. *J Biomed Opt* 2013; 18: 066018.
29. Nadort A, Kalkman K, van Leeuwen TG, et al. Quantitative blood flow velocity imaging using laser speckle flowmetry. *Sci Rep* 2016; 6: 25258.